



Changes in extreme precipitation in the Wei River Basin of China during 1957–2019 and potential driving factors

Dexun Qiu^{1,2} · Changxue Wu³ · Xingmin Mu^{1,3,2} · Guangju Zhao^{1,3,2} · Peng Gao^{1,3,2}

Received: 26 January 2022 / Accepted: 14 May 2022 / Published online: 23 May 2022
© The Author(s), under exclusive licence to Springer-Verlag GmbH Austria, part of Springer Nature 2022

Abstract

Extreme precipitation poses a severe threat to the natural ecosystem, socioeconomic development, and human life. Investigating the spatiotemporal variations in extreme precipitation and exploring the potential drivers have implications for disaster risk reduction and water resource management. In this study, we analyzed the changes in nine extreme precipitation indices (EPIs) over the Wei River Basin (WRB) during 1957–2019. Furthermore, we assessed the effect of geographic factors (latitude, longitude, and altitude) on the spatial distribution of EPIs and the potential impact of ocean–atmosphere circulation on the temporal variability of EPIs. The results indicate that six EPIs present a downward trend and three EPIs show an upward trend, but all the trends are not significant. In the seasonal scale, max 1-day precipitation amount (RX1day) increases significantly in summer ($P < 0.05$), while the trends in max 5-day precipitation amount (RX5day) are not significant in all seasons. The period of about 8 years and less than 3 years were observed in most EPIs. The mean values of EPIs except consecutive dry days (CDD) gradually increase from northwest to southeast of the WRB. Latitude, longitude, and altitude are important factors affecting the spatial distribution of the extreme precipitation. Southern Oscillation Index (SOI) and Atlantic Multidecadal Oscillation (AMO) contribute the most to EPIs variation. Interdecadal and interannual oscillations occur between most EPIs and ocean-atmospheric circulation factors, but their phase relationships are different. Our findings highlight the importance of examining global and local driving factors of trend in regional extreme precipitation by a systematic approach, and help to further understand the precipitation changes in the WRB.

1 Introduction

Global warming has accelerated the process of the hydrological cycle, leading to more frequent and severe extreme climate events (Diffenbaugh et al. 2017; Santos et al. 2011; Trenberth 2011). Compared to mean climatic values, it is

easier for extreme climate events to cause natural disasters such as flooding and drought disasters (IPCC 2013). These rain-induced disasters seriously threaten ecosystem and water resource security as well as production and life of human society (Papalexioiu and Montanari 2019). The situation is even acute in the developing countries where the population density is high and the drainage infrastructure is inadequate and imperfect (Croitoru et al. 2016). To better understand the characteristic of extreme climate events and reduce the damage caused by them, many studies on extreme precipitation at various spatial–temporal scales have been launched.

On the global scale, some studies have reported that the intensity and frequency of extreme precipitation have increased as the globe warms (Alexander et al. 2016; Donat et al. 2017; Westra et al. 2014). Meanwhile, Westra et al. (2014) further clarified that the change of extreme precipitation depends on the duration of the events and geographical location. On the regional scale, however, the trend of extreme precipitation varies considerably across regions (Li et al. 2020; Mass et al. 2011; Nayak et al. 2018; Panthou

✉ Xingmin Mu
xmmu@ms.iswc.ac.cn

✉ Peng Gao
gaopeng@ms.iswc.ac.cn

¹ State Key Laboratory of Soil Erosion and Dryland Farming On the Loess Plateau, Institute of Soil and Water Conservation, Chinese Academy of Sciences and Ministry of Water Resources, Yangling 712100, Shaanxi, China

² University of Chinese Academy of Sciences, Beijing 100049, China

³ State Key Laboratory of Soil Erosion and Dryland Farming On the Loess Plateau, Institute of Soil and Water Conservation, Northwest A&F University, Yangling 712100, Shaanxi, China

et al. 2014; Quan et al. 2021; Shao et al. 2019; Sheikh et al. 2014). In recent decade, there have been a growing body of studies suggesting the change of precipitation extremes in China's different regions. Similar to many regions of the world, these studies showed that the extreme precipitation exhibits obvious regional variations (Du et al. 2020; Fan et al. 2012; Wang et al. 2013, 2021; Zhang et al. 2014a). It has been reported that extreme precipitation events increased in southern and northwestern China and decreased in northern, central, and northeastern China (Li et al. 2015, 2020; Sun et al. 2016; Zhai et al. 2005). Deng et al. (2014) found that precipitation extremes such as number of heavy precipitation days and consecutive wet days have increased in northwest China. By contrast, a significant decrease in maximum 5-day precipitation amount and consecutive wet days was observed in Huang-Huai-Hai River basin of China (Zhang et al. 2015). Compared to global and continental scales, it is more necessary and feasible to investigate the change of extreme precipitation from a regional perspective (Li et al. 2018; You et al. 2011).

Previous studies have shown that the large-scale ocean–atmosphere circulation patterns such as El Niño–Southern Oscillation (ENSO) have profound effect on extreme precipitation. The extreme precipitation is affected by the combined effects of global warming and ENSO (Li et al. 2016a, 2018). Limsakul and Singhruck (2016) reported that ENSO and Pacific Decadal Oscillation (PDO) are two remote driving factors of the extreme precipitation change in Thailand. Large-scale circulation patterns may amplify or counteract the influences of global warming on precipitation extremes (Alexander et al. 2009; Kenyon and Hegerl 2010). Li et al. (2020) indicated that the regional response of extreme precipitation to global warming is uncertain and heterogeneous. In addition, geographical factors (e.g., latitude, longitude, elevation, land use, urbanization) further add uncertainty to the spatiotemporal variations in precipitation extremes (Ghosh et al. 2012; Mondal and Mujumdar 2015). Therefore, regional investigations of spatiotemporal variations in extreme precipitation and analysis of its potential driving factors are needed for helping us understand and predict extreme precipitation events.

The Wei River Basin (WRB)—the largest tributary of the Yellow River Basin (YRB—as experienced highly frequent droughts and floods in history (Huang et al. 2015). Since the twenty-first century, extreme precipitation events occurred frequently in the WRB. For instance, there were six heavy precipitation events from August to October 2003 that lasted over 50 days. A large-scale continuous precipitation lasted from September to October 2005 across the whole basin. However, the WRB has suffered severe droughts in 2007 and 2014 (Zou et al. 2021). Frequent and intense extreme precipitation events seriously threaten the industrial and agricultural production of the WRB (Qiu et al. 2022). Moreover,

frequent heavy rainfall in summer is one of the important causes of soil erosion on the Loess Plateau in the northern part of the WRB (Liu et al. 2017; Sun et al. 2016). The comprehensive research of changes in extreme precipitation in the WRB is needed for climate disasters monitoring and preventing. Most current studies focus on investigating the spatial–temporal variability of extreme precipitation in the WRB (Jiang et al. 2019; Liu et al. 2017; Qiu et al. 2022); however, the relationship between extreme precipitation and potential driving factors is not clear. Additionally, with the update of the data, re-examining the trend of extreme precipitation is necessary for responding to the climate change and adjusting the strategies accordingly (Li et al. 2020). Our primary objects here are to (1) investigate the spatial–temporal variation of nine EPIs in the WRB and (2) explore the relationship between potential driving factors (geographical factors and ocean–atmospheric circulation factors) and extreme precipitation variability. This regional study will contribute to provide reliable information for disaster prevention and mitigation, agricultural sustainable development and ecological protection.

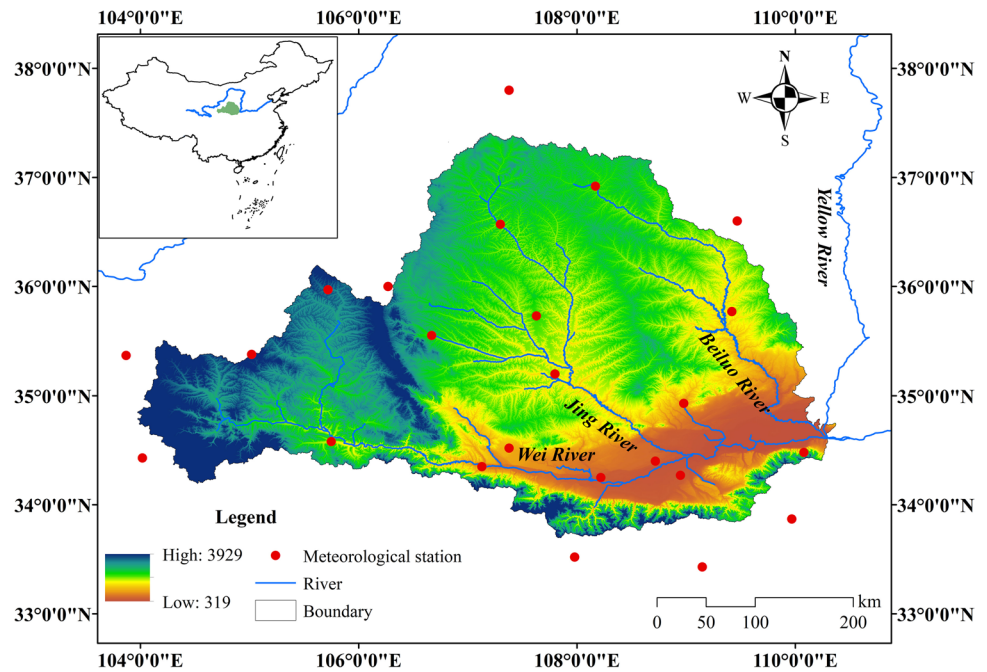
2 Materials and methods

2.1 Study area

The Wei River Basin (WRB) (Fig. 1)—with a length of 818 km and a drainage area of 135 000 km²—is located in the Midwest of China. The WRB originates from the north of Niaoshu Mountain in Gansu Province and flows from Tianshui, Baoji, Xianyang, Xi'an, Weinan cities into the Yellow River in Tongguan County in Shaanxi Province. The Jing River (JR) and Beiluo River (BLR) are two main tributaries of Wei River (WR). The northern part of the WRB is Loess Plateau, and the southern part is Qinling Mountains. The WRB is one of the most economically developed regions in Northwest China where agricultural production is high as well as commercial and industrial are flourishing. Moreover, the WRB is an important source for drinking water, directly supporting more than 22 million people.

The WRB is situated in a semi-dry and semi-humid monsoon climate zone, characterized by hot-rainy summers and cold-dry winters. Because of the complex landform and diverse climate conditions, the meteorological and hydrological features of the WRB vary greatly in different seasons and regions (Li et al. 2016b). The annual precipitation of the WRB is approximately 570 mm (averaged for the period of 1981–2010). About 60% of the annual precipitation falls from June to September (Fan et al. 2017). The mean annual temperature ranges from 7.8 to 13.5 °C, and the mean annual potential evapotranspiration is between 800 and 1200 mm (Chang et al. 2014). The mean annual runoff

Fig. 1 Study area and meteorological station locations



is approximately 10 billion m³, accounting for 17.3% of total runoff in the Yellow River (Jiang et al. 2019).

2.2 Data sources

2.2.1 Precipitation

Daily precipitation data recorded from 24 surface meteorological stations of the WRB and its surrounding area during the period 1957–2019 were obtained from the China Meteorological Data Service Center (CMDC) (<http://data.cma.cn/>). The distribution of these stations is shown in Fig. 1. To ensure the completeness and consistency of data, we removed the stations which percentage of annual missing data more than 10%. The short-term missing precipitation values (less than 2 days) were interpolated by the average values of the same day from adjacent stations. The missing values more than 2 days were replaced by -99.9 . A homogeneity test was performed to the precipitation series before the analysis. Finally, we used RCLimDex software package (Zhang and Feng 2004) for data quality checking.

2.2.2 Ocean-atmospheric circulation indicators

In view of the influence of ocean–atmosphere circulation on extreme precipitation, eight ocean–atmosphere circulation indices were chosen to reveal the relationship between climate change and extreme precipitation in the WRB. The eight ocean–atmosphere circulation indices include Niño3.4, Southern Oscillation Index (SOI),

Pacific Decadal Oscillation (PDO), North Pacific pattern (NP), North Atlantic Oscillation (NAO), Arctic Oscillation (AO), Atlantic Multidecadal Oscillation (AMO), and Western Pacific Index (WPI). These indices have been used extensively in previous studies (e.g., Liu et al. 2017; Limsakul and Singhruck 2016; Wang et al. 2021).

ENSO is a significant signal of global climate change. ENSO refers to both El Niño and La Niña phenomena, which is generally considered as the result of dramatic temperature changes in the Eastern Pacific. Niño3.4 and SOI are two important indices for the representation of ENSO (Kiem and Franks 2001; Ward et al. 2016). ENSO is proven to interact with other atmospheric oscillations, such as PDO (Wang et al. 2017). The PDO index is defined as the leading standardized principal component of monthly SST anomalies in the North Pacific. The AMO index is based on the average anomalies of SST in the North Atlantic basin. PDO and AMO have a great impact on climate change in China (Han et al. 2018). The NP index, which is the area-weighted sea level pressure, is used to measure interannual to decadal variations in the atmospheric circulation. NAO, AO, and WPI are low-frequency modes of the atmosphere, which play an important role in climate change in the Northern Hemisphere (Liu et al. 2017; Wang et al. 2021).

The above indices are obtained from the Earth System Research Laboratory of the Physical Sciences Division National Oceanic and Atmospheric Administration of the United States (<https://www.esrl.noaa.gov/psd/data/climateindices/list/>).

3 Method

3.1 EPIs

In this study, nine EPIs recommended by the Expert Team on Climate Change Detection and Indices (ETCCDI) (<http://cccma.seos.uvic.ca/ETCCDI>) were selected (Table 1). We classified these indices into four categories: (1) intensity-based index (RX1day, RX5day, and SDII); (2) quantity-based index (R95P and PRCPTOT); (3) frequency-based index (R10mm and R20mm); (4) duration-based index (CDD and CWD).

3.2 Trend analysis

The non-parametric Mann–Kendall (M–K) trend test (Kendall 1948; Mann 1945) was used to analyze trends of EPIs. Although the M–K trend test has been recommended by the World Meteorological Organization (WMO) and used extensively, it fails to eliminate the effect of autocorrelation. This problem will increase the probability of occurrence of the significant level (Von Storch 1995). Therefore, we adopted the method of trend-free pre-whitening (TFPW) to pre-processing data (Kulkarni and Von Storch 1995; Von Storch 1995), removing the autocorrelation in original time series. A M–K trend test was used for the new sequence after the process of TFPW. Statistical parameter Z was calculated for measuring the trend significance. When Z is positive, the trend is increasing, and when it is negative, the trend is decreasing. When the absolute value of Z is larger than 1.96 and 2.58, the time series has a significant trend at 0.05 and 0.01 significance level, respectively.

3.3 Wavelet transforms

3.3.1 The continuous wavelet transform (CWT)

The wavelet transform was first proposed by Morlet et al. (1982) which overcame the deficiency of traditional Fourier transform. This technique has been extensively used to analyze sequence containing non-stationary power at many different frequencies. The CWT of time series is its convolution with the local basis functions, or wavelets, which can be stretched and translated with flexible resolution in both frequency and time (Jevrejeva et al. 2003). The CWT of the time series d regarding the wavelet ψ is defined as follows:

$$W_{d,\psi}(s, t) = (d(t) * \psi_s(t)) \quad (1)$$

where s denotes wavelet scale, t is time, and $*$ represents the complex conjugate. The wavelet power is defined as $|W_{d,\psi}(s)|^2$. However, the CWT has edge artifacts due to the wavelet is not completely localized in time (Grinsted et al. 2004). The Cone of Influence (COI) was thus be introduced as an area in which edge effects cannot be ignored and is defined as the e-folding time for the autocorrelation of wavelet power at each scale (Su et al. 2019). In this study, a Morlet wavelet was used as a wavelet basis function due to its excellent localization property. Statistical significance was estimated against a red noise model (Torrence and Compo 1998).

3.3.2 Wavelet coherence (WTC)

WTC can be regarded as the local correlation between two CWTs, which reveals areas with high common power. In this way, local phase locked behavior is detected (Grinsted et al. 2004). The WTC of two series $X = (x_1, x_2, \dots, x_n)$ and $Y = (y_1, y_2, \dots, y_n)$ is defined as follows:

Table 1 List of nine EPIs used in this study

Index	Indicator name	Definition	Units
RX1day	Max 1-day precipitation amount	Maximum 1-day precipitation amount	mm
RX5day	Max 5-day precipitation amount	Maximum 5-day precipitation amount	mm
R95P	Very wet days	Annual total precipitation from days with RR > 95th percentile	mm
R10mm	Number of heavy precipitation days	Annual count of days with RR \geq 10 mm	days
R20mm	Number of very heavy precipitation days	Annual count of days with RR \geq 20 mm	days
PRCPTOT	Annual total wet-day precipitation	Annual total precipitation from days with RR > 1 mm	mm
SDII	Simple precipitation intensity index	The ratio of annual total wet-day precipitation to the number of wet days	mm day ⁻¹
CDD	Consecutive dry days	Maximum number of consecutive days with RR < 1 mm	days
CWD	Consecutive wet days	Maximum number of consecutive days with RR \geq 1 mm	days

RR denotes daily precipitation amount

$$R_n^2(s) = \frac{|S(S^{-1}W_n^{XY}(s))|^2}{S(|S^{-1}W_n^X(s)|^2) \cdot S(|S^{-1}W_n^Y(s)|^2)}, \quad (2)$$

where S is a smoothing operator, expressed as follows:

$$S(W) = S_{scale}(S_{time}(W_n(s))), \quad (3)$$

where S_{scale} represents smoothing along the wavelet scale axis and S_{time} smoothing in time. The value of R_n^2 is between zero and one, inclusively. The closer R_n^2 is to one, the stronger the correlation between two time series. The 5% statistical significance level of the wavelet coherence is determined using Monte Carlo methods. More detailed information about WTC is described by Grinsted et al. (2004). Herein, the ability of different atmosphere–ocean signals to explain extreme precipitation variation was evaluated by calculating the mean wavelet transform coherence.

The relevant codes for the procedures of CWT and WTC are available online (<http://noc.ac.uk/using-science/cross-wavelet-wavelet-coherence>).

3.4 Factor identifying

The ability of different ocean–atmosphere circulation factors to explain EPIs variations was assessed through determining average wavelet coherence (AWC) and the percent area of significant coherence (PASC). A higher AWC with greater PASC indicates that more variations in EPIs are explained by a specific ocean–atmosphere circulation factor (Su et al. 2019). In this way, we could identify the potential driving factors underlying the changes in EPIs. Notice that the increase of independent variables sometimes increases AWC, but does not necessarily increase the PASC (Hu and Si 2013). The increase in the PASC indicates a significant increase in EPIs changes, which can be explained at a significant level of 95%. In other words, a factor is considered significant when it causes the PASC to increase by at least 5% (Hu and Si 2013; Su et al. 2019).

4 Results and discussion

4.1 Trends in EPIs

The trends of nine EPIs over the WRB during the period of 1957–2019 are shown in Fig. 2. The CDD and CWD exhibit decreases at rate of -0.70 day decade $^{-1}$ and -0.16 day decade $^{-1}$, respectively (Fig. 2a–b). The average PRCPTOT is about 525.09 mm, with downward trend at -5.89 mm decade $^{-1}$ (Fig. 2c). In addition, the 5-year moving average line indicates that the decreasing trend in PRCPTOT mainly occurs during 1991–1997 (Fig. 2c). Our results here are

consistent with Feng et al. (2018) and Zou et al. (2021), who pointed out downward trend in the average annual precipitation over the WRB, and the main period of decline was concentrated in the early 1990s. Sun et al. (2016) found that the eastern Asian summer monsoon was weaker in 1986–2013 compared with 1960–1985. During this period, the westerly jet and any southwest flow from the ocean weakened, resulting in a short rainy season in northern China (You et al. 2011), which may explain the decreasing trend in PRCPTOT. Similarly, the R10mm, RX5day, and SDII show decreasing trends at rate of -0.12 day decade $^{-1}$, -0.45 mm decade $^{-1}$ and -0.01 mm day $^{-1}$ decade $^{-1}$, respectively (Fig. 2d, h, and i). By comparison, the regionally averaged R20mm, R95P, and RX1day increase from 1957 to 2019 at rate of 0.10 day decade $^{-1}$, 0.64 day decade $^{-1}$, and 0.17 mm decade $^{-1}$, respectively (Fig. 2e, f, and g). These results indicate EPIs with a downward trend are more than that with an upward trend, though all the trends are not statistically significant, which may be one of the reasons for the reduction of soil erosion and sediment transport in this region (Miao et al. 2010).

To further reveal seasonal differences in EPIs across the WRB, we explored the seasonal variation of RX1day and RX5day (Fig. 3). RX1day shows a significant upward trend in summer at rate of 0.57 mm decade $^{-1}$ ($P < 0.05$), while it does not present a significant trend in other seasons (Fig. 3a). The seasonal trends of RX5day are analogous to RX1day, but not significant in each season (Fig. 3b). Moreover, the increasing trends of RX1day and RX5day both occur in summer and winter, while the decreasing trends both occur in spring and autumn. This is good agreement with the finding on the temporal change of precipitation in the WRB by Zhao et al. (2015), who reported that increasing trend occurred in summer and winter. The risk of flooding and drought will be intensified due to the uneven precipitation throughout seasons in the WRB (Wang et al. 2021).

The spatial distribution of the trends of these EPIs in all stations is shown in Fig. 4. As shown in Fig. 4, more stations in the WRB are negative trends dominated for five EPIs, i.e., CWD, PRCPTOT, R10mm, R20mm, and RX5day. The other four EPIs including CDD, R95P, RX1day, and SDII are increasing trends dominated. For each EPI, there are no more than three stations exhibit a statistically decreasing or increasing trend ($P < 0.05$). These results are generally in line with Jiang et al. (2019), though their research period is 1969–2016.

4.2 Wavelet analysis of EPIs

Figure 5 shows the CWT results for nine EPIs. The thick black contours represent the 0.05 significance level against red noise and the pale regions denote the COI. Significant periodicities characteristics were found in all EPIs. A strong periodicity of approximately 5–7 years and a slight

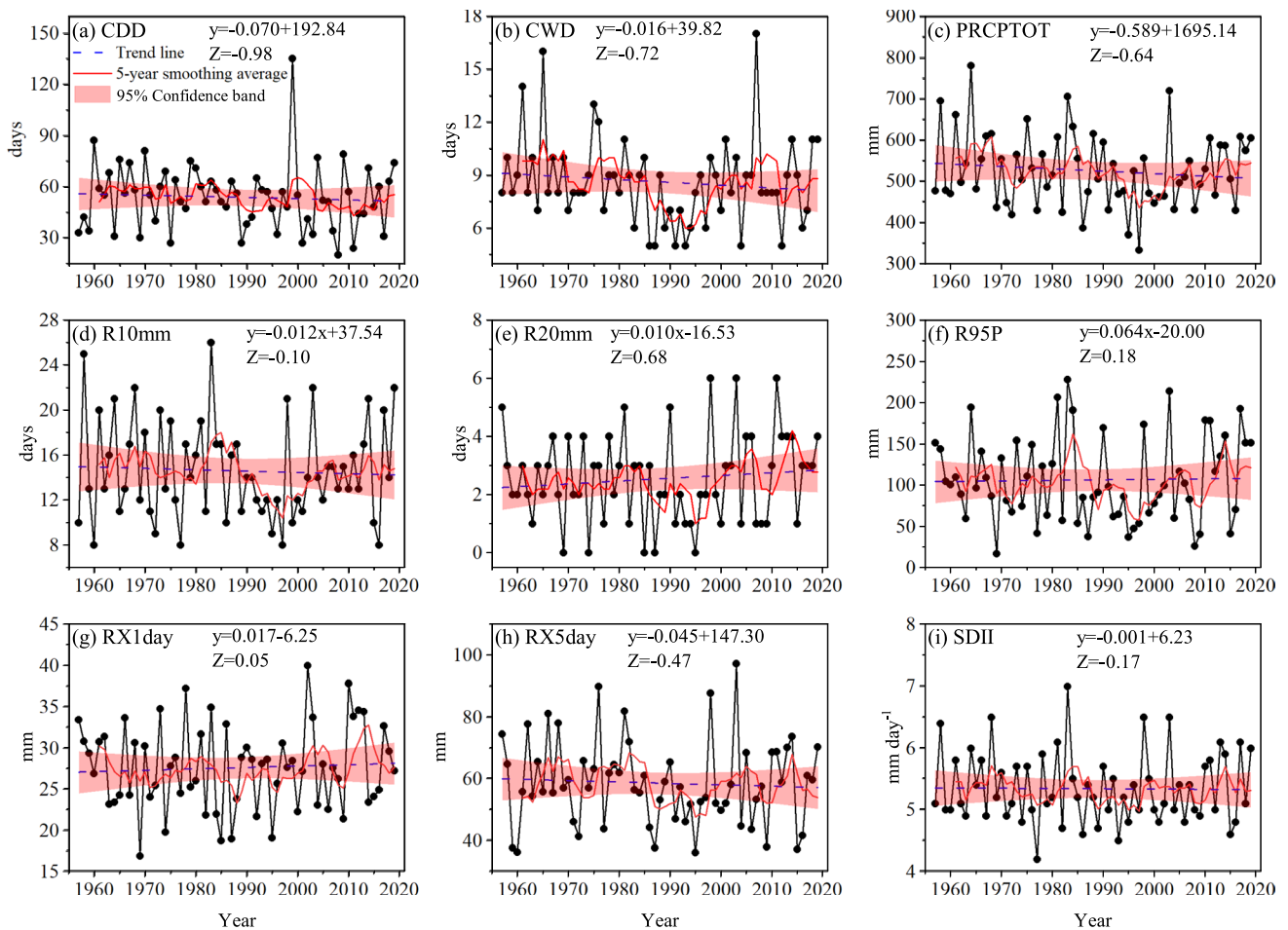


Fig. 2 Trends in nine EPIs across the WRB during 1957–2019. **a** CDD. **b** CWD. **c** PRCPTOT. **d** R10mm. **e** R20mm. **f** R95P. **g** RX1day. **h** RX5day. **i** SDII

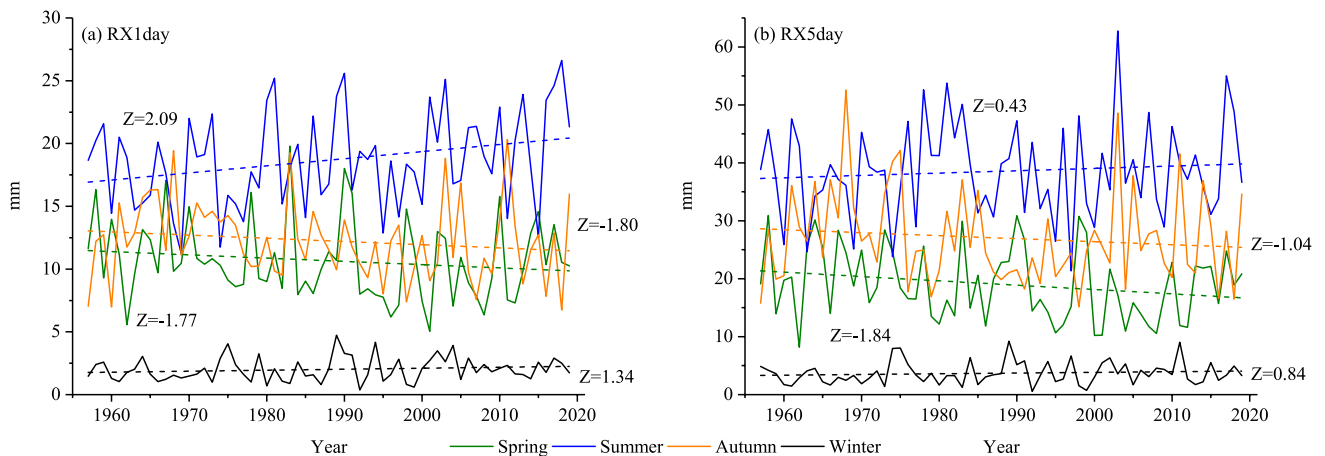


Fig. 3 Seasonal variation in **a** RX1day and **b** RX5day across the WRB during 1957–2019

periodicity of 1–2 years were observed for CDD during 1990–2010 and 1995–2000, respectively. The CWD shows a 7-year oscillation (2005–2010) and a periodicity of less

than one year during 1960s. Two periodicities including approximately 5 years during 1980s and 1 to 3 years during 1960s were revealed in PRCPTOT. Only one periodicity of

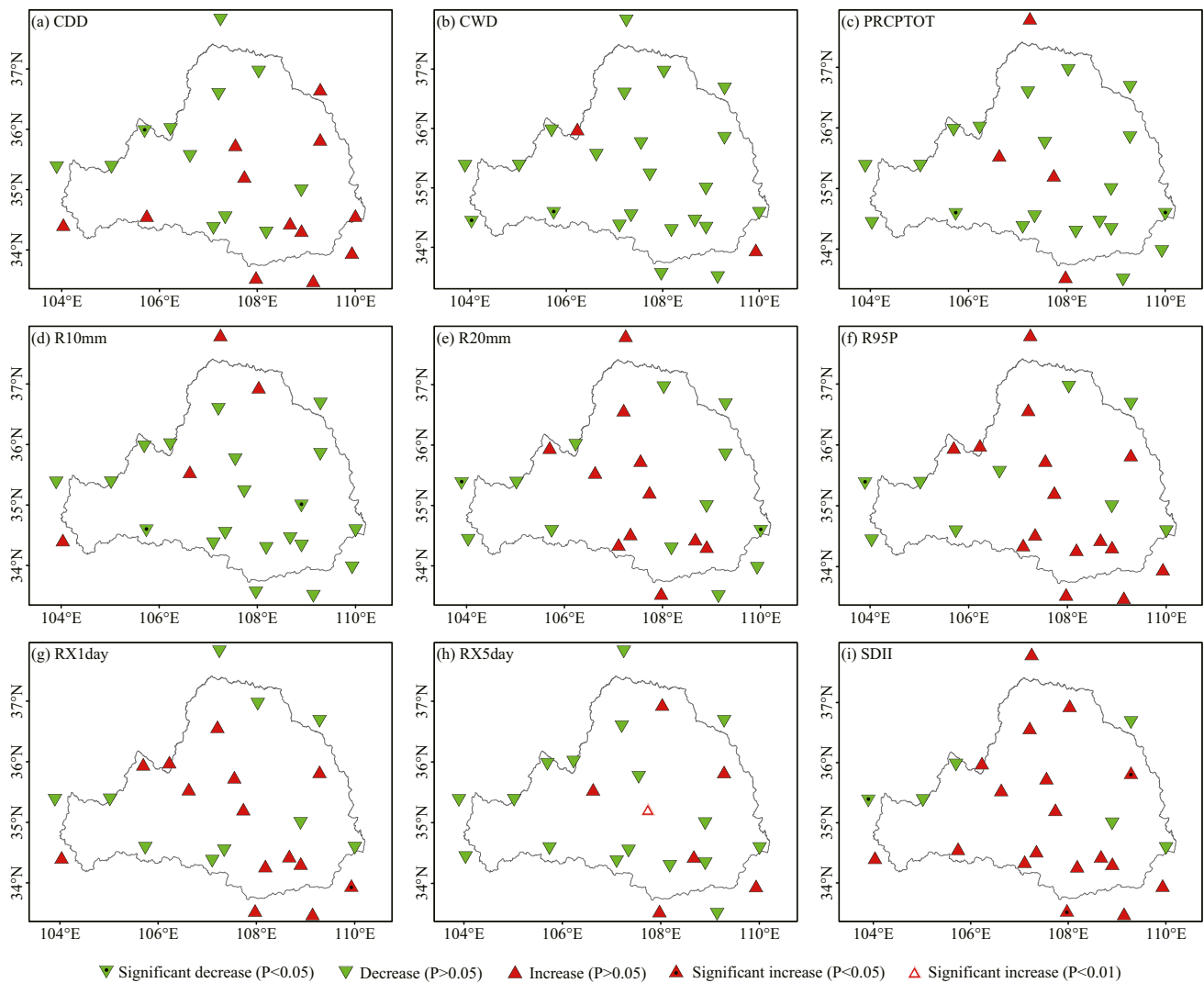


Fig. 4 Spatial patterns of trends in nine EPIs across the WRB during 1957–2019. **a** CDD. **b** CWD. **c** PRCPTOT. **d** R10mm. **e** R20mm. **f** R95P. **g** RX1day. **h** RX5day. **i** SDII

1 to 3 years was observed in R10mm during the 1960s. Four periodicities were observed in R20mm, including two oscillations of 1–2 years during 1970s and 1980s and one oscillation of 4 years (about 2000) and about 8 years (1990–2010). The CWT reveals a common feature of R95P, RX1day, and RX5day, they both have three remarkable oscillations. They display a periodicity of less than 3 years during 1980–1985, 1970s–1980s, and about 2000, respectively. Meanwhile, R95P and RX1day show two approximately 8-year oscillations (1980s and about 2010) and a 7- to 15-year oscillation (1997–2015), respectively. Additionally, RX1day and RX5day display a periodicity of approximately 5 years (about 2000). For SDII, the CWT show four periodicities including two oscillations of less than 3 years during 1980s and about 2010, and two oscillations of 4–7 years and approximately 16 years during 1990s and 1980s,

respectively. In general, most EPIs show an oscillation of less than 3 years and a period of about 8 years. These results are basically consistent with previous studies conducted on precipitation extremes in the upper reaches of the Yellow River (Ma and Gao 2019).

4.3 Spatial variability of EPIs

The probability density curves of nine EPIs across the stations in the WR, JR, and BLR is shown in Fig. 6. The CDD of the WR is significantly lower than that of the JR and BLR ($P < 0.05$); for CWD, PRCPTOT, R10mm, and R20mm, however, the WR is significantly higher than the JR and BLR ($P < 0.05$). For R95P, the WR and BLR are significantly higher than the JR ($P < 0.01$). Nevertheless, the RX1day, RX5day, and SDII of the

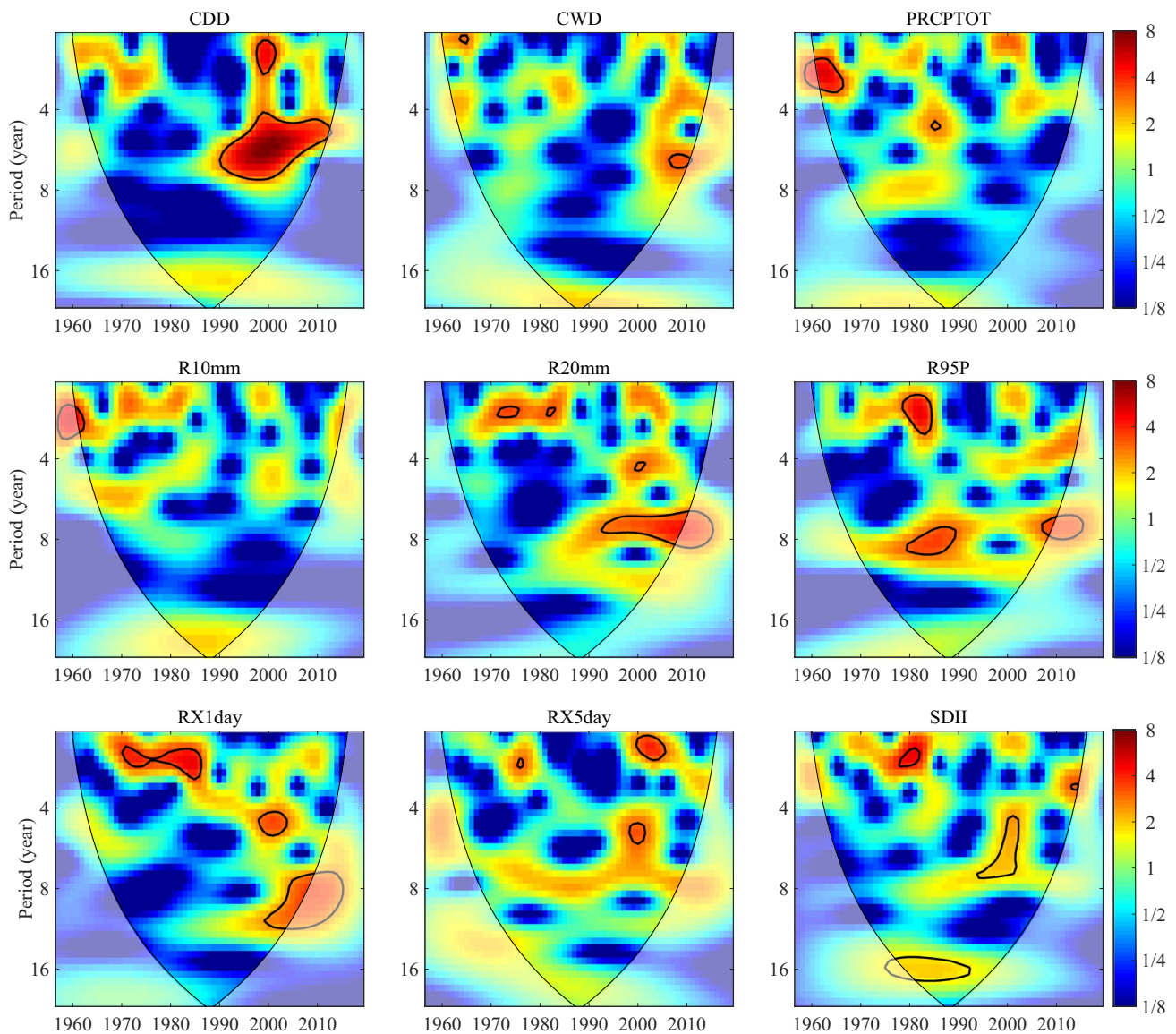


Fig. 5 Continuous wavelet transforms for nine EPIs series. The period is measured in months. Thick contours denote 5% significance levels against red noise. Pale regions denote the cone of influence

where edge effects might distort the results. The color denotes the strength of wavelet power

BLR are significantly higher than that of the WR and JR ($P < 0.05$). The intensive extreme precipitation over the BLR easily triggers the soil erosion (Liu et al. 2017). As shown in Fig. 7, all EPIs with high values are found in the southeast of the basin except for CDD, though the distribution scope are slightly different. We concluded that EPIs (except for CDD) of the WRB gradually increase from northwest to southeast, which is consistent with that in Liu et al. (2017) and Zou et al. (2021). In addition, an interesting phenomenon is observed, showing the capital city Xi'an and its surrounding cities have relative low mean values of EPIs (indicated by PRCPTOT, R10mm,

R20mm, R95P, RX1day, and RX1day). Most previous studies have shown that rapid urbanization will increase the intensity and frequency of extreme precipitation (Fu et al. 2019; Liang and Ding 2017; Wu et al. 2019), which seems to contradict our results. However, as found by Kaufmann et al. (2007), urbanization reduces precipitation in the Pearl River Delta of China. This reduction may be due to changes in surface hydrology that extend beyond the urban heat island effect (Kishtawal et al. 2010; Limsakul and Singhruck 2016) and energy-related aerosol emissions (Zhang 2020). This may account for lower values of EPIs in Xi'an city.

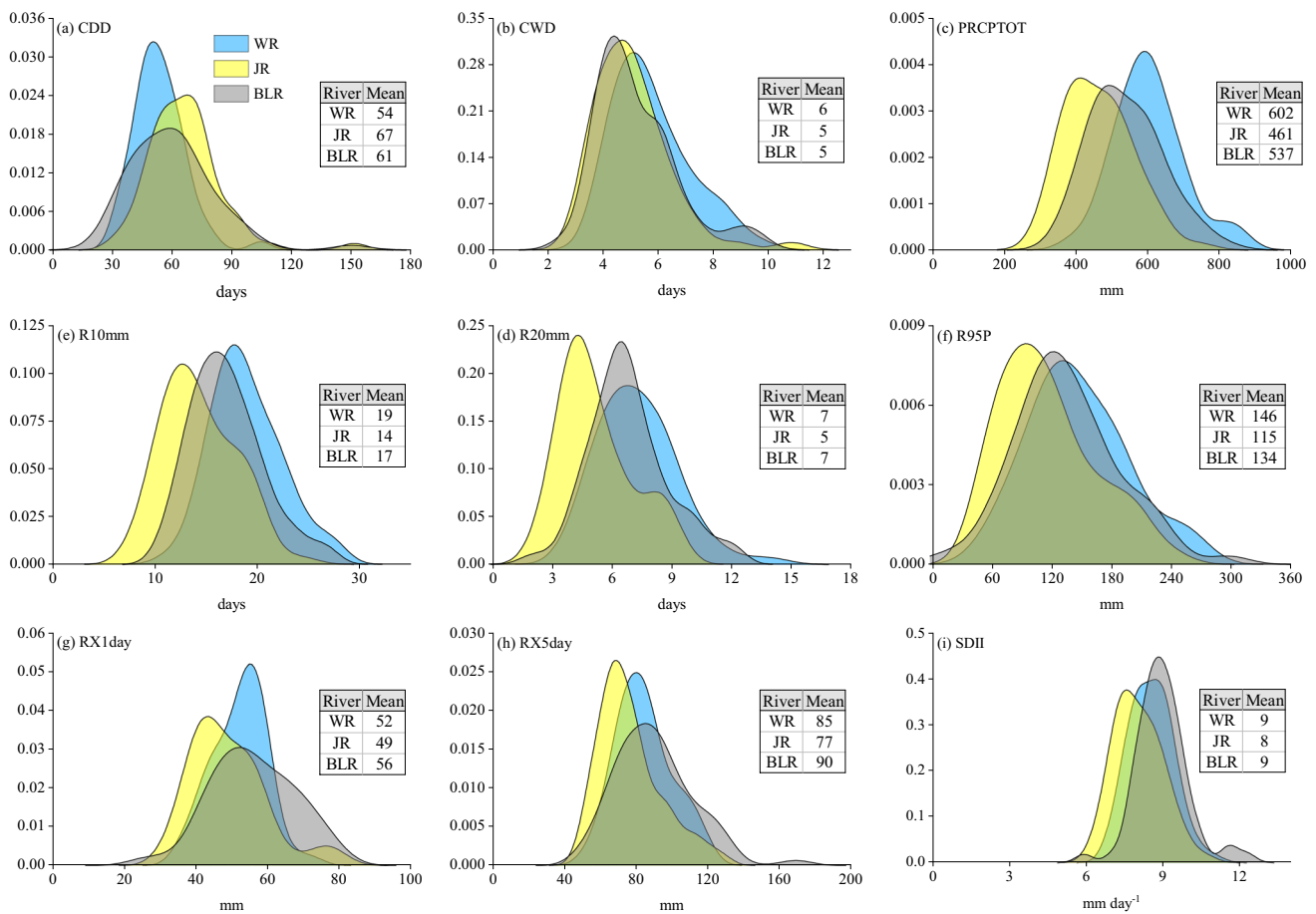


Fig. 6 Probability density curves of EPIs across the stations in the Wei River (WR), Jing River (JR), and Beiluo River (BLR). The mean value of the index is listed in a table alongside the density

plot. **a** CDD. **b** CWD. **c** PRCPTOT. **d** R10mm. **e** R20mm. **f** R95P. **g** RX1day. **h** RX5day. **i** SDII

4.4 The relationship between EPIs and geographic factors

The effect of geographical factors (latitude, longitude, and altitude) on spatial distribution of the climatology of EPIs is shown in Table 2. In order to highlight the most important variables of each index, the factors with the highest correlation are displayed in bold. There is a significant negative correlation between EPIs (except for CDD) and latitude ($P < 0.05$). However, the EPIs (except for CDD) and longitude is significantly positively correlated ($P < 0.05$). These results suggest that latitude and longitude are important factors affecting spatial variability of EPIs in the WRB. Climate warming has intensified the difference in the thermal properties between land and sea (IPCC 2013). This further enhance the relationship between precipitation and latitude as well as longitude. Altitude plays a noticeable role in the redistribution of water vapor and heat, and then affects the precipitation in mountainous areas. Here, all EPIs are negatively correlated with altitude except for

CDD. Furthermore, we divided altitude into three ranges including < 1000 m, $1000\text{--}1500$ m, and > 1500 m to explore the linkage between extreme precipitation and altitude at different range across the WRB. Most EPIs (except for CDD) are positively correlated with altitude at less than 1000 m, while these indices are negatively correlated with altitude at $1000\text{--}1500$ m. When the altitude is higher than 1500 m, the correlation between most EPIs and altitude is weak and irregular (Table 2). The cause of the difference may derive from the propagation direction of the water vapor flux varies with altitude gradients (Zhang et al. 2014b). As pointed by Fu. (1995), precipitation on the windward slope will increase with altitude at first and then decrease after attaining a height of maximum precipitation. However, the influence of altitude on precipitation was relatively complex. Local climatic conditions could strongly influence the relationship between topography and the spatial distribution of precipitation (Basist et al. 1994). Meanwhile, we noted that the correlation between most indices (except for RX1day and SDII) and altitude decrease when the altitude of more than

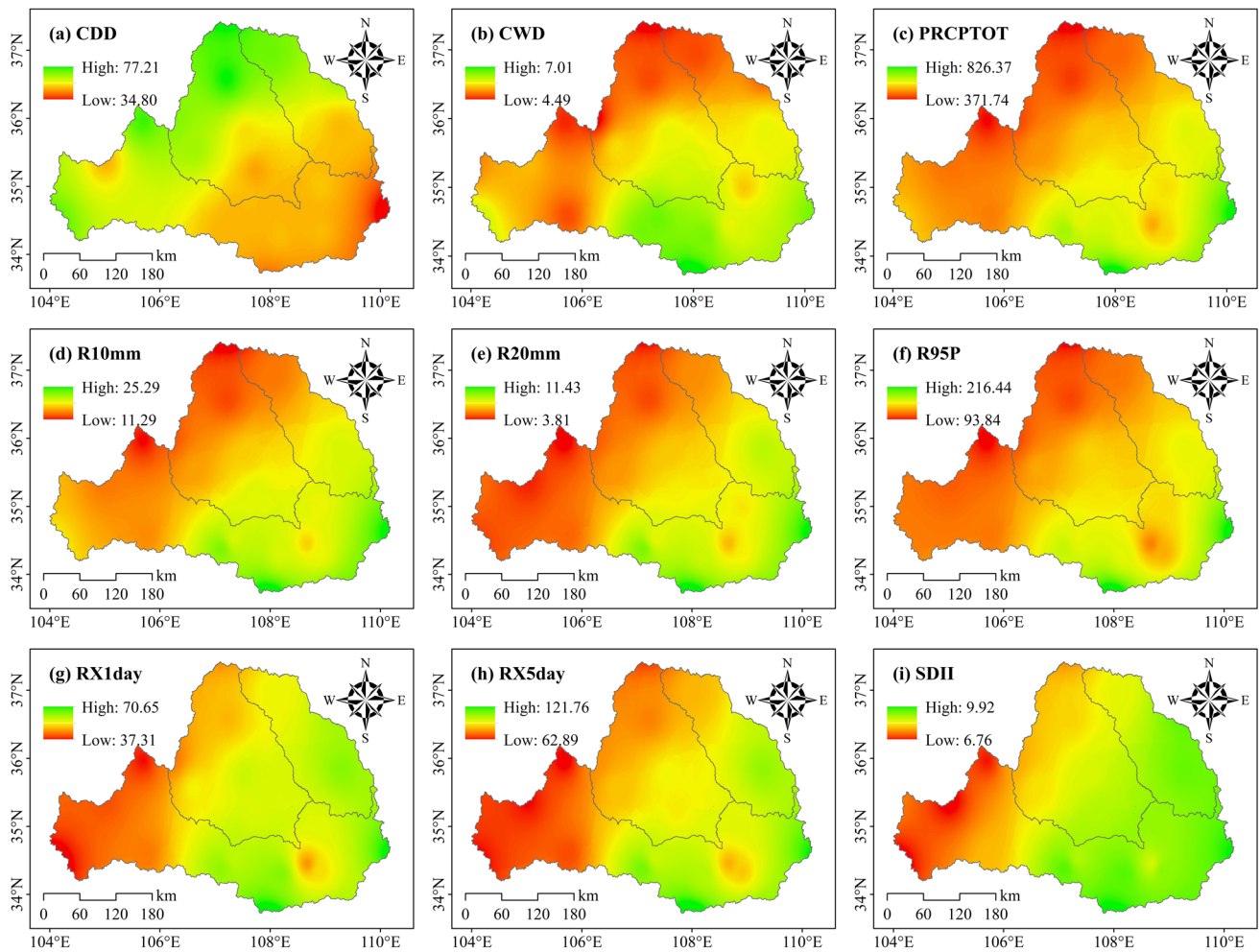


Fig. 7 Spatial distribution characteristic of nine EPIs across the WRB during 1957–2019. **a** CDD. **b** CWD. **c** PRCPTOT. **d** R10mm. **e** R20mm. **f** R95P. **g** RX1day. **h** RX5day. **i** SDII

Table 2 Correlation between EPIs and latitude, longitude, and altitude

Index	Latitude	Longitude	Altitude			
			< 2500 m (24)	< 1000 m (10)	1000–1500 m (8)	> 1500 m (6)
CDD	0.773**	−0.516**	0.311	−0.014	0.388	−0.251
CWD	−0.827**	0.302	−0.325	0.150	−0.132	0.608
PRCPTOT	−0.787**	0.443*	−0.298	0.469	−0.344	0.188
R10mm	−0.815**	0.447*	−0.338	0.446	−0.370	0.196
R20mm	−0.694**	0.611**	−0.461*	0.444	−0.313	−0.089
R95P	−0.699**	0.505*	−0.320	0.527	−0.267	0.079
RX1day	−0.423*	0.687**	−0.491*	0.533	−0.033	−0.140
RX5day	−0.572**	0.652**	−0.492*	0.563	−0.156	−0.184
SDII	−0.500**	0.795**	−0.692**	0.418	−0.323	−0.331

* is significant at the 0.05 level, ** is significant at the 0.01 level

1500 m, indicating that the influence of altitude on extreme precipitation was weakened.

Besides natural geographical factors, human activities such as urbanization (Gu et al. 2019), land use (Zhao and

Pitman 2002), and aerosol emission (Wild et al. 2008) could also influence precipitation formation and local microclimates, thus influence extreme precipitation. Future work should comprehensively consider these local factors to

examine the cause of the extreme precipitation changes. Also, a large-scale ocean–atmosphere circulation is of momentous and complex impacts on changes in extreme precipitation events, which will be discussed in next section.

4.5 Teleconnection between EPIs and ocean–atmosphere circulation

Table 3 and Table 4 summarize the effect of ocean–atmosphere circulation factors on EPIs changes. From Table 3, it can be found that AWC between EPIs and ocean–atmosphere circulation factors is relatively low in general. Among the eight factors, SOI is the most common influencing factors, accounting for the highest variation coherence for three EPIs (PRCPTOT, RX1day, and RX5day). PDO, AMO, and WPI are next in importance, with the highest coherence for two EPIs. NP, Niño3.4, NAO, and AO have lower impact on EPIs variation. As shown in Table 4, similar to AWC, it is found that the PASC presents low as a whole. AMO is the dominant ocean–atmosphere circulation factor with

the highest PASC for three EPIs (PRCPTOT, R95P, and RX1day). Next in importance is SOI, which has the highest PASC for two EPIs (RX5day and SDII). PDO, NP, AO, and WPI accounts for the highest PASC for one EPI. Niño3.4 and NAO have lower impact on EPIs variation. Although the factor with the highest AWC is not completely consistent with the factor with the highest PASC, SOI and AMO contribute the most to EPIs variation in general, followed by PDO and WPI. As point by Liu et al. (2017), extreme precipitation in the WRB is more greatly affected by ENSO events than PDO. Some documents have indicated that PDO has an indirect influence on precipitation change through modulating ENSO (Kiem and Verdon-Kidd 2009; Verdon et al. 2004). In addition, Li et al. (2020) found a predominant positive correlation pattern between EPIs and ENSO index of the preceding year. Given the uncertainty of the potential interactions between ENSO events and other large-scale circulation patterns (Kiem and Verdon-Kidd 2009), the underlying mechanisms on both spatial and temporal scales need to be further explored.

Table 3 AWC between EPIs and ocean–atmosphere circulation factors

Index	SOI	PDO	NP	Niño3.4	NAO	AO	AMO	WPI
CDD	0.349	0.358	0.361	0.344	0.288	0.335	0.338	0.368
CWD	0.300	0.243	0.316	0.323	0.272	0.282	0.270	0.448
PRCPTOT	0.470	0.369	0.400	0.391	0.305	0.391	0.425	0.298
R10mm	0.435	0.367	0.425	0.353	0.314	0.381	0.448	0.349
R20mm	0.367	0.427	0.437	0.302	0.320	0.382	0.382	0.242
R95P	0.423	0.483	0.464	0.344	0.318	0.377	0.448	0.255
RX1day	0.431	0.357	0.393	0.347	0.347	0.382	0.394	0.321
RX5day	0.528	0.356	0.416	0.422	0.275	0.324	0.308	0.452
SDII	0.385	0.353	0.396	0.340	0.301	0.341	0.413	0.355

AWC refers to average wavelet coherence. Values are the mean wavelet coherence at significant locations across all scales and times. Entries in bold indicate the factor with the highest AWC. *SOI*, Southern Oscillation Index; *PDO*, Pacific Decadal Oscillation; *NP*, North Pacific pattern; *NAO*, North Atlantic Oscillation; *AO*, Arctic Oscillation; *AMO*, Atlantic Multidecadal Oscillation; *WPI*, Western Pacific Index

Table 4 PASC (%) for the wavelet transform coherence between EPIs and ocean–atmosphere circulation factors

Index	SOI	PDO	NP	Niño3.4	NAO	AO	AMO	WPI
CDD	7.82	8.84	1.36	1.36	2.53	1.88	4.08	7.67
CWD	4.38	2.19	2.04	0.11	3.21	2.41	2.53	11.03
PRCPTOT	9.37	3.09	6.23	7.70	2.19	0.51	15.79	0.49
R10mm	8.23	5.17	8.57	7.67	1.32	14.85	14.47	1.81
R20mm	3.81	13.79	14.13	2.38	2.45	11.56	1.96	0.68
R95P	7.02	16.47	15.53	6.23	3.51	10.84	15.68	0.37
RX1day	10.2	12.16	12.32	1.70	6.76	8.76	21.54	2.87
RX5day	22.10	1.36	11.82	13.26	0.00	8.80	1.88	8.95
SDII	10.58	1.05	5.70	2.79	0.86	6.84	5.32	5.47

PASC refers to the percent area of significant coherence relative to the whole wavelet scale–time domain at all locations at various scales (outside the cone of influence). Entries in bold indicate the factor with the highest PASC. *SOI*, Southern Oscillation Index; *PDO*, Pacific Decadal Oscillation; *NP*, North Pacific pattern; *NAO*, North Atlantic Oscillation; *AO*, Arctic Oscillation; *AMO*, Atlantic Multidecadal Oscillation; *WPI*, Western Pacific Index

Figure 8 depicts the WTC results for EPIs and the factor that best explains variations in each index. It is noteworthy that significant coherence between two signals does not necessarily mean that the powers of the two signals are also statistically significant (Rathinasamy et al. 2019). As shown in Fig. 8, we can find the periods of high coherence, weakening coupling or even the absence of significant coupling between EPIs and ocean–atmosphere circulation factors. Here, we only focus the periods of high coherence of the two signals. Interdecadal oscillations are shown in most wavelet coherence plots, but their phase relationships were not identical.

For example, there is a significant coherence at the 5% level between CDD and PDO at the scale of around 18 years, with an almost in-phase (positive correlation) during 1980–1995. However, about a 10- to 16-year significant oscillation at the 5% level was detected between RX1day and AMO, with RX1day leading AMO by about 90° ($2.5\text{--}4$ years) during 1985–2005. Besides, SOI leads SDII by about 135° during 1980s and 1990s, which means that SDII lags behind SOI by around 5.8–7.4 years. The remarkable interannual covariance was observed in all wavelet coherence plots with varying phase differences. For example, there is a

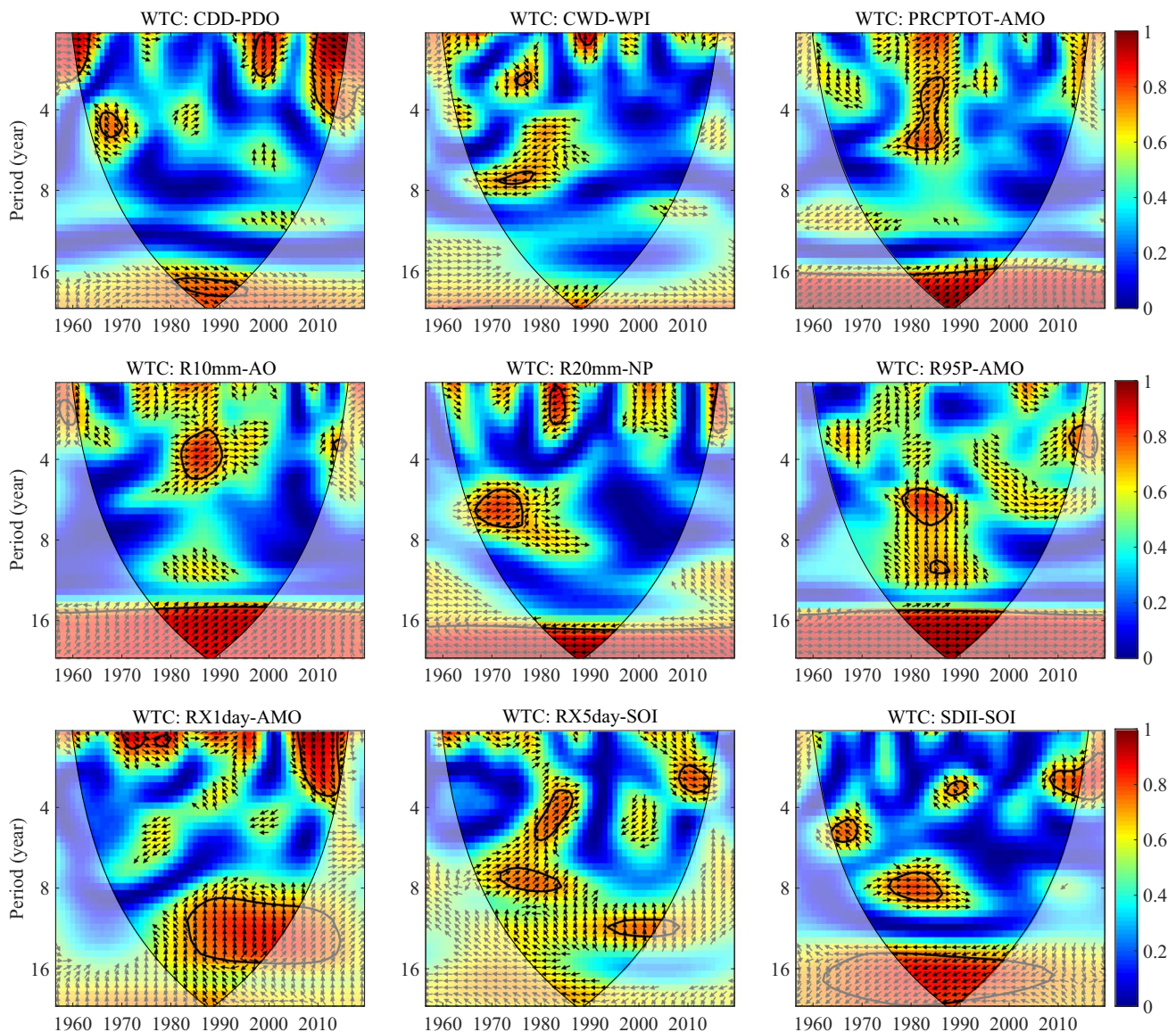


Fig. 8 Wavelet transform coherence between EPIs and ocean–atmosphere circulation factors. The period is measured in years. Thick contours denote 5% significance levels against red noise. Pale regions denote the cone of influence where edge effects might distort the results. Small arrows denote the relative phase relationship (in-phase,

arrows point right; anti-phase, arrows point left). The color denotes the strength of coherence. SOI, Southern Oscillation Index; PDO, Pacific Decadal Oscillation; NP, North Pacific pattern; NAO, North Atlantic Oscillation; AO, Arctic Oscillation; AMO, Atlantic Multi-decadal Oscillation; WPI, Western Pacific Index

significant coherence at the 5% level between CDD and PDO at the scale of less than three years (about 2000) and 1–6 years (2005–2015). PDO leads CDD by about 45° (0.13–0.75 years) during 2005–2015. There is an almost in-phase (positive correlation) relationship between R20mm and NP during 1970s. We also found an in-phase (positive correlation) relationship between RX5day/SDII and SOI. A strong periodicity ($P < 0.05$) of approximately 7 years was observed between CWD and WPI during 1970s, with an anti-phase (positive correlation) relationship. In general, the area of significant coherence at the 5% level between CWD and WPI on the interannual timescale is extremely limited, indicating a slight relation between them. PRCP-TOT/R10mm leads AMO/AO by around 45° (approximately 0.25–0.75 years) during 1980s, while R95P leads AMO by about 45° (~0.75 years). Besides, two strong periodicities ($P < 0.05$) of approximately 2–6 years and 8 years between RX5day and SOI were detected during 1970–1985, in which RX5day leads SOI by about 45°. Similarly, two strong periodicities ($P < 0.05$) of approximately 4–6 years and 2–4 years between SDII and AO were observed during 1965–1970 and about 1990, with SDII leading AO by about 135°.

Our findings demonstrate the importance of considering different time scales when exploring the impact of ocean–atmosphere circulation on regional extreme precipitation. Compared to the traditional method of correlation analysis (e.g., Pearson correlation analysis), wavelet coherence analysis can comprehensively reflect the changing relations between extreme precipitation and ocean–atmospheric circulation. Although the WRB is chosen as the case study for this work, the approach applied here is suitable for similar and even smaller regions.

5 Conclusions

This study presented a comprehensive analysis of changes in nine EPIs recommended by the ETCCDI in the WRB during 1957–2019. The effect of three geographical factors (i.e., latitude, longitude, and altitude) and large-scale ocean–atmosphere circulation on extreme precipitation changes were detected. The main conclusions can be summarized as follows.

1. Six EPIs including CDD, CWD, PRCP-TOT, R10mm, RX5day, and SDII show a decreasing trend and three EPIs including R20mm, R95P, and RX1day show an increasing trend, but all the trends are insignificant. RX1day increases significantly in summer ($P < 0.05$) while the trends in RX5day are not significant in all seasons.
2. All EPIs exhibit significant periodicity characteristics, and most EPIs generally show an oscillation of about eight years and a period of less than 3 years.

3. The mean values of EPIs (except for CDD) gradually increase from northwest to southeast of the WRB. However, in Xi'an and its surrounding cities, the mean values of most EPIs are relatively low. The extreme precipitation intensity (indicated by RX1day, RX5day, and SDII) of the BLR is significantly higher than that of the WR and JR ($P < 0.05$).

4. Latitude, longitude, and altitude significantly affect the spatial distribution of EPIs. Latitude is negatively associated with EPIs (except for CDD), while longitude is positively correlated with them. Altitude has complicated impact on extreme precipitation, and it may take different roles under different altitude gradient.

5. Ocean–atmosphere circulation factors include SOI and AMO contribute the most to the temporal variation of EPIs, PDO, and WPI are also important drivers of EPIs change. Interdecadal and interannual oscillations occur between EPIs and ocean–atmospheric circulation indices, but their phase relationships are different.

These findings highlight the importance of systematically studying the global and local drivers of regional extreme precipitation trends, and could contribute to better understand and predict the extreme precipitation in the WRB. However, the driving factors of extreme precipitation change are diverse and complex. The accurate interpretation for the driving mechanism of extreme precipitation change at different scales in the context of global warming still remains a notable challenge. Future study should consider additional influencing factors and focus on the prediction of regional extreme precipitation events using climate models. Additionally, it is necessary to further investigate the hydrological responses to extreme precipitation and thoroughly assess the potential risks.

Author contribution Peng Gao: conceptualization, supervision. Dexun Qiu: methodology, software, writing—original draft, visualization. Changxue Wu: writing—original draft, writing—reviewing, and editing, data curation. Xingmin Mu and Guangju Zhao: writing—reviewing. All authors read and approved the final manuscript.

Funding This work was supported by the National Key Research and Development Program of China (Grant No. 2017YFE0118100-1).

Data availability The meteorological observations are archived by the China Meteorological Administration. The ocean–atmospheric circulation indicators are provided by the Earth System Research Laboratory of the Physical Sciences Division National Oceanic and Atmospheric Administration of the United States.

Code availability The RCLimDex software package and the codes for the procedures of CWT and WTC, used in this study are available from the corresponding author upon request.

Declarations

Ethics approval The authors paid attention to the ethical rules in the study. There is no violation of ethics.

Consent to participate All the authors admitted that they have contributed to the study.

Consent for publication If this study is accepted, it can be published in the *Theoretical and Applied Climatology* journal.

Conflict of interest The authors declare no competing interests.

References

- Alexander LV, Uotila P, Nicholls N (2009) Influence of sea surface temperature variability on global temperature and precipitation extremes. *J Geophys Res* 114:D18116
- Alexander LV, Zhang X, Peterson TC, Caesar J, Gleason B, Klein Tank AMG, Haylock M, Collins D, Trewin B, Rahimzadeh F, Tagipour A, Rupa Kumar K, Revadekar J, Griffiths G, Vincent L, Stephenson DB, Burn J, Aguilar E, Brunet M, Taylor M, New M, Zhai P, Rusticucci M, Vazquez-Aguirre JL (2016) Global observed changes in daily climate extremes of temperature and precipitation. *J Geophys Res* 111:D05109
- Basist A, Bell GD, Meentemeyer V (1994) Statistical relationships between topography and precipitation patterns. *J Clim* 7:1305–1315
- Chang JX, Wang YM, Istanbuluoglu E, Bai T, Huang Q, Yang DW, Huang SZ (2014) Impact of climate change and human activities on runoff in the Weihe River Basin, China. *Quatern Int* 380–381:169–179
- Croitoru AE, Piticar A, Burada DC (2016) Changes in precipitation extremes in Romania. *Quatern Int* 415:325–335
- Deng HJ, Chen YN, Shi X, Li WH, Wang HJ, Zhang SH, Fang GH (2014) Dynamics of temperature and precipitation extremes and their spatial variation in the arid region of northwest China. *Atmos Res* 138:346–355
- Diffenbaugh NS, Singh D, Mankin JS, Horton DE, Swain DL, Touma D, Charland A, Liu Y, Haugen M, Tsiang M (2017) Quantifying the influence of global warming on unprecedented extreme climate events. *Proc Natl Acad Sci U S A* 114:4881–4886
- Donat MG, Lowry AL, Alexander LV, O’Gorman PA, Maher N (2017) More extreme precipitation in the world’s dry and wet regions. *Nat Clim Change* 7:154–158
- Du MC, Zhang JY, Yang QL, Wang ZL, Bao ZX, Liu YL, Jin JL, Liu CS, Wang GQ (2020) Spatial and temporal variation of rainfall extremes for the North Anhui Province Plain of China over 1976–2018. *Nat Hazards* 105:1–21
- Fan XH, Wang QX, Wang MB (2012) Changes in temperature and precipitation extremes during 1959–2008 in Shanxi, China. *Theor Appl Climatol* 109:283–303
- Fan JJ, Huang Q, Liu DF (2017) Identification of impacts of climate change and direct human activities on streamflow in Weihe River Basin in Northwest China. *Int J Agr Biol Eng* 10:119–129
- Feng X, Guo JQ, Sun DY, Cao Y (2018) Climate change characteristics in Weihe River Basin from 1960 to 2015. *Arid Land Geogr* 41:718–725 (**in Chinese**)
- Fu B (1995) The effects of orography on precipitation. *Bound-Lay Meteorol* 75:189–205
- Fu XS, Yang XQ, Sun XG (2019) Spatial and diurnal variations of summer hourly rainfall over three super city clusters in eastern China and their possible link to the urbanization. *J Geophys Res* 124:5445–5462
- Ghosh S, Das D, Kao SC, Ganguly AR (2012) Lack of uniform trends but increasing spatial variability in observed Indian rainfall extremes. *Nat Clim Change* 2:86–91
- Grinsted A, Moore JC, Jevrejeva S (2004) Application of the cross wavelet transform and wavelet coherence to geophysical time series. *Nonlinear Proc Geoph* 11:561–566
- Gu XH, Zhang Q, Li JF, Singh VP, Sun P (2019) Impact of urbanization on nonstationarity of annual and seasonal precipitation extremes in China. *J Hydrol* 575:638–655
- Han TT, He SP, Hao X, Wang HJ (2018) Recent interdecadal shift in the relationship between Northeast China’s winter precipitation and the North Atlantic and Indian Oceans. *Clim Dyn* 50:1413–1424
- Hu W, Si BC (2013) Soil water prediction based on its scale-specific control using multivariate empirical mode decomposition. *Geoderma* 193:180–188
- Huang SZ, Hou BB, Chang JX, Huang Q, Chen YT (2015) Spatial-temporal change in precipitation patterns based on the cloud model across the Wei River Basin, China. *Theor Appl Climatol* 120:391–401
- IPCC (2013) Summary for policymakers. In: *Climate Change 2013: The Physical Science Basis. Contribution of Working Group to the Fifth Assessment Report of the Intergovernmental Panel on Climate Change*. Cambridge University Press, Cambridge, UK; New York, NY, USA.
- Jevrejeva S, Moore JC, Grinsted A (2003) Influence of the Arctic Oscillation and El Niño-Southern Oscillation (ENSO) on ice conditions in the Baltic Sea: the wavelet approach. *J Geophys Res* 108. <https://doi.org/10.1029/2003JD003417>
- Jiang RG, Wang YP, Xie JC, Zhao Y, Li FW, Wang XJ (2019) Assessment of extreme precipitation events and their teleconnections to El Niño Southern Oscillation, a case study in the Wei River Basin of China. *Atmos Res* 218:372–384
- Kaufmann RK, Seto KC, Schneider A, Liu ZT, Zhou LM, Wang WL (2007) Climate response to rapid urban growth: evidence of a human-induced precipitation deficit. *J Clim* 20:2299–2306
- Kendall MG (1948) *Rank Correlation Methods*. Griffin, London
- Kenyon J, Hegerl GC (2010) Influence of modes of climate variability on global precipitation extremes. *J Clim* 23:6248–6262
- Kiem AS, Franks SW (2001) On the identification of ENSO-induced rainfall and runoff variability: a comparison of methods and indices. *Hydrol Sci J* 46:715–727
- Kiem AS, Verdon-Kidd DC (2009) Climatic drivers of Victorian streamflow: is ENSO the dominant influence? *Aust J Water Resour* 13:17–29
- Kishtawal CM, Niyogi D, Tewari M, Pielke RA, Shepherd JM (2010) Urbanization signature in the observed heavy rainfall climatology over India. *Int J Climatol* 30:1908–1916
- Kulkarni A, Von Storch H (1995) Monte Carlo experiments on the effect of serial correlation on the Mann-Kendall test of trend. *Meteorol Z* 4:82–85
- Li YG, He DM, Hu JM, Cao J (2015) Variability of extreme precipitation over Yunnan Province, China 1960–2012. *Int J Climatol* 35:245–258
- Li X, Meshgi A, Babovic V (2016a) Spatio-temporal variation of wet and dry spell characteristics of tropical precipitation in Singapore and its association with ENSO. *Int J Climatol* 36:4831–4846
- Li YY, Chang JX, Wang YM, Jin WT, Guo AJ (2016) Spatiotemporal impacts of climate, land cover change and direct human activities on runoff variations in the Wei River Basin. *China Water* 8:220
- Li X, Wang X, Babovic V (2018) Analysis of variability and trends of precipitation extremes in Singapore during 1980–2013. *Int J Climatol* 38:125–141
- Li X, Zhang K, Gu PR, Feng HT, Yin YF, Wang C, Cheng BC (2020) Changes in precipitation extremes in the Yangtze River Basin during 1960–2019 and the association with global warming, ENSO, and local effects. *Sci Total Environ* 760:144244

- Liang P, Ding YH (2017) The long-term variation of extreme heavy precipitation and its link to urbanization effects in Shanghai during 1916–2014. *Adv Atmos Sci* 34:321–334
- Limsakul A, Singhruck P (2016) Long-term trends and variability of total and extreme precipitation in Thailand. *Atmos Res* 169:301–317
- Liu SY, Huang SZ, Huang Q, Xie YY, Leng GY, Luan JK, Song XY, Wei X, Li XY (2017) Identification of the non-stationarity of extreme precipitation events and correlations with large-scale ocean-atmospheric circulation patterns: a case study in the Wei River Basin, China. *J Hydrol* 548:184–195
- Ma JN, Gao YH (2019) Analysis of annual precipitation and extreme precipitation change in the upper Yellow River Basin in recent 50 years. *Plateau Meteorol* 38:124–135 ((in Chinese))
- Mann HB (1945) Nonparametric tests against trend. *Econometrica* 245–259
- Mass C, Skalenakis A, Warner M (2011) Extreme precipitation over the west coast of North America: Is there a trend? *J Hydrometeorol* 12:310–318
- Miao C, Ni J, Borthwick AG (2010) Recent changes of water discharge and sediment load in the Yellow River basin, China. *Prog Phys Geogr* 34:541–561
- Mondal A, Mujumdar PP (2015) Modeling non-stationarity in intensity, duration and frequency of extreme rainfall over India. *J Hydrometeorol* 521:217–231
- Morlet J, Arens G, Fourgeau E, Giard D (1982) Wave propagation and sampling theory; Part II, Sampling theory and complex waves. *Geophysics* 47:222–236
- Nayak S, Dairaku K, Takayabu I, Suzuki-Parker A, Ishizaki NN (2018) Extreme precipitation linked to temperature over Japan: current evaluation and projected changes with multi-model ensemble down-scaling. *Clim Dyn* 51:4385–4401
- Panthou G, Vischel T, Lebel T (2014) Recent trends in the regime of extreme rainfall in the Central Sahel. *Inter J Climatol* 34:3998–4006
- Papalexiou SM, Montanari A (2019) Global and regional increase of precipitation extremes under global warming. *Water Resour Res* 55:4901–4914
- Qiu DX, Wu CX, Mu XM, Zhao GJ, Gao P (2022) Spatial-temporal analysis and prediction of precipitation extremes: a case study in the Weihe River Basin, China. *Chin Geogra Sci* 32:358–372
- Quan NT, Khoi DN, Hoan NX, Phung NK, Dang TD (2021) Spatiotemporal trend analysis of precipitation extremes in Ho Chi Minh City, Vietnam during 1980–2017. *Inter J Disaster Risk Sci* 11(5):131–146
- Rathinasamy M, Agarwal A, Sivakumar B, Marwan N, Kurths J (2019) Wavelet analysis of precipitation extremes over India and teleconnections to climate indices. *Stoch Env Res Risk A* 33:2053–2069
- Santos CACD, Neale CMU, Rao TVR, Silva BBD (2011) Trends in indices for extremes in daily temperature and precipitation over Utah, USA. *Inter J Climatol* 31:1813–1822
- Shao YT, Mu XM, He Y, Sun WY, Zhao GJ, Gao P (2019) Spatiotemporal variations of extreme precipitation events at multi-time scales in the Qinling-Daba mountains region, China. *Quatern Int* 525:89–102
- Sheikh MM, Manzoor N, Ashraf J, Adnan M, Collins D, Hameed S, Manton MJ, Ahmed AU (2014) Trends in extreme daily rainfall and temperature indices over South Asia. *Inter J Climatol* 35:1625–1637
- Su L, Miao CY, Duan QY, Lei XH, Li H (2019) Multiple-wavelet coherence of world's large rivers with meteorological factors and ocean signals. *J Geophys Res* 124:4932–4954
- Sun WY, Mu XM, Song XY, Wu D, Cheng AF, Qiu B (2016) Changes in extreme temperature and precipitation events in the Loess Plateau (China) during 1960–2013 under global warming. *Atmos Res* 168:33–48
- Torrence C, Compo GP (1998) A practical guide to wavelet analysis. *B Am Meteorol Soc* 79:61–78
- Trenberth KE (2011) Changes in precipitation with climate change. *Clim Res* 47:123–138
- Verdon DC, Wyatt AM, Kiem AS, Franks SW (2004) Multidecadal variability of rainfall and streamflow: Eastern Australia. *Water Resour Res* 40:W10201
- Von Storch H (1995) Misuses of statistical analysis in climate research. In: von Storch, H., Navarra, A. (Eds.), *Analysis of Climate Variability*, Springer, Berlin, Heidelberg.
- Wang BL, Zhang MJ, Wei JL, Wang SJ, Li XF, Li SS, Zhao AF, Li XS, Fan JP (2013) Changes in extreme precipitation over Northeast China, 1960–2011. *Quatern Int* 298:177–186
- Wang LY, Chen SF, Zhu WB, Ren H, Zhang LJ, Zhu LQ (2021) Spatiotemporal variations of extreme precipitation and its potential driving factors in China's North-South Transition Zone during 1960–2017. *Atmos Res* 252:105429
- Wang C, Deser C, Yu JY, Dinezio P, Clement A (2017) El Niño and southern oscillation (ENSO): a review. In *Coral reefs of the eastern tropical Pacific* (pp. 85–106). Springer, Dordrecht.
- Ward PJ, Kumm M, Lall U (2016) Flood frequencies and durations and their response to El Niño Southern Oscillation: Global analysis. *J Hydrol* 539:358–378
- Westra S, Fowler HJ, Evans JP, Alexander LV, Berg P, Johnson F, Kendon EJ, Lenderink G, Roberts NM (2014) Future changes to the intensity and frequency of short-duration extreme rainfall. *Rev Geophys* 52:522–555
- Wild M, Grieser J, Schär C (2008) Combined surface solar brightening and increasing greenhouse effect support recent intensification of the global land-based hydrological cycle. *Geophys Res Lett* 35(17): <https://doi.org/10.1029/2008GL034842>.
- Wu MW, Luo YL, Chen F, Wong WK (2019) Observed link of extreme hourly precipitation changes to urbanization over coastal south China. *J Appl Meteorol Clim* 58:1799–1819
- You Q, Kang S, Aguilar E, Pepin N, Flügel WA, Yan Y, Xu Y, Zhang Y, Huang J (2011) Changes in daily climate extremes in China and their connection to the large scale atmospheric circulation during 1961–2003. *Clim Dyn* 36:2399–2417
- Zhai PM, Zhang XB, Wan H, Pan XH (2005) Trends in total precipitation and frequency of daily precipitation extremes over China. *J Clim* 18:1096–1108
- Zhang DL (2020) Rapid urbanization and more extreme rainfall events. *Sci Bull* 65:516–518
- Zhang X, Feng Y (2004) RCLimDex (1.0) user manual. Climate Research Branch Environment Canada Downs View, Ontario
- Zhang KX, Pan SM, Cao LG, Wang Y, Zhao YF, Zhang W (2014) Spatial distribution and temporal trends in precipitation extremes over the Hengduan Mountains region, China, from 1961 to 2012. *Quatern Int* 349:346–356
- Zhang Q, Xiao MZ, Li JF, Singh VP, Wang ZZ (2014) Topography-based spatial patterns of precipitation extremes in the Poyang Lake basin, China: changing properties and causes. *J Hydrol* 512:229–239
- Zhang D, Yan D, Wang Y, Lu F, Wu D (2015) Changes in extreme precipitation in the Huang-Huai-Hai River basin of China during 1960–2010. *Theor Appl Climatol* 120:195–209
- Zhao M, Pitman AJ (2002) The impact of land cover change and increasing carbon dioxide on the extreme and frequency of maximum temperature and convective precipitation. *Geophys Res Lett* 29:2-1-2–4
- Zhao AZ, Zhu XF, Liu XF, Pan YZ (2015) Spatial and temporal variation of precipitation in Weihe River Basin from 1965 to 2013. *J Nat Resour* 30:1896–1909 ((in Chinese))
- Zou L, Yu JY, Wang FY, Zhang Y (2021) Spatial-temporal variations of extreme precipitation indices and their response to atmospheric circulation factors in the Weihe River Basin. *Arid Zone Res* 38:764–774 ((in Chinese))
- Zuo DP, Xu ZX, Wu W, Zhao J, Zhao FF (2014) Identification of streamflow response to climate change and human activities in the Wei River Basin, China. *Water Resour Manag* 28:833–885

Publisher's note Springer Nature remains neutral with regard to jurisdictional claims in published maps and institutional affiliations.